Journal of Inorganic Biochemistry 197 (2019) 110721

Contents lists available at ScienceDirect

Journal of Inorganic Biochemistry

journal homepage: www.elsevier.com/locate/jinorgbio

Inhibitory effects of oxidovanadium complexes on the aggregation of human islet amyloid polypeptide and its fragments

Jufei Xu, Baohong Zhang, Gehui Gong, Xiangyi Huang, Weihong Du*

Department of Chemistry, Renmin University of China, Beijing 100872, China

ARTICLE INFO

Keywords:
hIAPP
hIAPP19-37
hIAPP20-29
Aggregation
Oxidovanadium complexes
Inhibition

ABSTRACT

Human islet amyloid polypeptide (hIAPP) is synthesized by pancreatic β-cells and co-secreted with insulin. Misfolding and amyloidosis of hIAPP induce β-cell dysfunction in type II diabetes mellitus. Numerous small organic molecules and metal complexes act as inhibitors against amyloid-related diseases, justifying the need to explore the inhibitory mechanism of these compounds. In this work, three oxidovanadium complexes, namely, $(NH_4)[VO(O_2)_2(bipy)]\cdot 4H_2O$ (**1**) (bipy = 2,2' bipyridine), bis(ethyl-maltolato, *O*,*O*)oxido-vanadium(IV) (**2**), and $(bipyH_2)H_2[O\{VO(O_2)(bipy)\}_2]\cdot 5H_2O$ (**3**), were synthesized and used to inhibit the aggregation of hIAPP and its fragments, namely, hIAPP19–37 and hIAPP20–29. Results revealed that shortening the peptide sequence decreased the aggregation capability of hIAPP fragments, and the oxidovanadium complexes inhibited the fibrillization of hIAPP better than its fragments. Interestingly, the binding of oxidovanadium complexes to hIAPP and its fragments presented a distinct thermodynamic behavior. Oxidovanadium complexes featured the disaggregation capability against hIAPP, better than against its fragments. These complexes also decreased the cytotoxicity caused by hIAPP and its fragments by reducing the production of oligomers. **3** may be a good hIAPP inhibitor based on its inhibition, disaggregation capability, and regulatory effect on peptide-induced cytotoxicity. Oxidovanadium complexes exhibit potential as metallodrugs against amyloidosis-related diseases.

1. Introduction

Human islet amyloid polypeptide (hIAPP, amylin) is a 37-residue polypeptide with a disulfide bond between residues Cys2 and Cys7 and is co-secreted by insulin-producing pancreatic β-cells in response to insulin release [1]. Misfolding and self-assembly transform hIAPP into an insoluble amyloid fibril, which causes β-cell dysfunction and decreases insulin release in type II diabetes mellitus (T2DM) [2,3]. T2DM is a chronic metabolic disease characterized by hyperglycemia caused by abnormal insulin secretion; new medications to treat this disease are still emerging [4–6]. hIAPP is involved in regulating the blood sugar balance associated with insulin. However, hIAPP may lose its natural structure and misfold, resulting in the pathological process of T2DM [7,8]. Therefore, hIAPP becomes a crucial target in T2DM treatment.

Inhibitors of hIAPP amyloid include organic aromatic compounds, short peptides, metal complexes, and nanoparticles [9–12]. Metal complexes, including Cu, Zn, and vanadium compounds, are currently applied in the inhibition of hIAPP and other amyloidosis related proteins [13–19]. Vanadium complexes have been used to test the anti-diabetes effects for > 100 years [20]. Bis(maltolato) oxovanadium (BMOV), bis(ethyl-maltolato, *O*,*O*)oxidovanadium(IV) (BEOV), $NaVO_3$, and other newly synthesized vanadium complexes lower blood glucose levels, enhance the quality of pancreatic cells, and lessen the need for daily insulin injections [21–29]. Several studies indicate that vanadium complexes exhibit distinct inhibitory effects against amyloid fibril formation of prion protein (PrP) fragments [15,18,30]. Nevertheless, the inhibitory effects of vanadium complexes against hIAPP and its fragments are rarely reported [31,32].

hIAPP fibrillation is a critical factor that induces β-cell apoptosis and T2DM, and the mechanism of fibril formation is complicated. The self-assembly of amyloid peptides generally includes the transformation of α-helix or random coil to β-sheet, oligomers, profibrils, and mature fibrils [33–37]. hIAPP aggregation depends on the hydrophobic hIAPP20–29 fragment, which is involved in the formation of the β-sheet-rich core region and shows strong tendency to form amyloid fibrils [38–40]. Numerous hIAPP fragments, such as 8–20, 20–29, 28–37, and 30–37, participate in amyloidogenic aggregation [39,41–43]. The N-terminal residues of hIAPP do not contribute to fibril formation but play a role in maintaining the stability of the amyloidogenic region [44]. hIAPP consists of the main amyloidogenic region 20–29 and the N-terminal fragment of hIAPP1–19, which is a superior binding region for insulin and membrane-disrupting sites. The C-terminal region

* Corresponding author.
E-mail address: whdu@ruc.edu.cn (W. Du).

https://doi.org/10.1016/j.jinorgbio.2019.110721
Received 12 March 2019; Received in revised form 26 April 2019; Accepted 13 May 2019
Available online 16 May 2019
0162-0134/

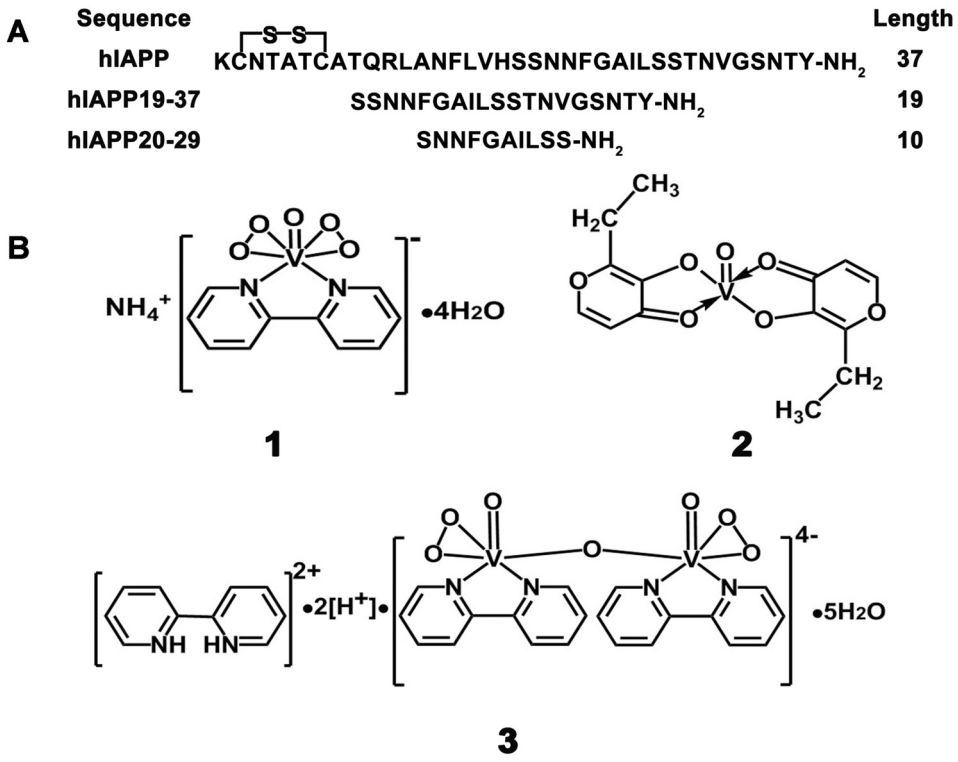

Scheme 1. (A) Sequence of hIAPP, hIAPP19-37, and hIAPP20-29. (B) Molecular structures of $(NH_4)[VO(O_2)_2(bipy)]\cdot 4H_2O$ (**1**), bis(ethyl-maltolato, *O,O*)oxidovanadiu-m(IV), (**2**), and $(bipyH_2)H_2$ $[O\{VO(O_2)(bipy)\}_2]\cdot 5H_2O$ (**3**).

hIAPP30-37 significantly enhances amyloid formation [45]. The cytotoxicity and membrane damage induced by hIAPP occur before amyloid formation [34,46]. Thus, exploring the interaction mechanisms between potential inhibitors and different hIAPP fragments are crucial for understanding the properties of these peptides.

This work investigated the aggregation behavior of different hIAPP fragments, namely, hIAPP19–37, hIAPP20–29, and the full length hIAPP1-37, affected by oxidovanadium complexes $(NH_4)[VO(O_2)_2(bipy)]\cdot 4H_2O$ (**1**) (bipy = 2,2' bipyridine), BEOV (**2**), and $(bipyH_2)H_2[O\{VO(O_2)(bipy)\}_2]\cdot 5H_2O$ (**3**) (Scheme 1). Dynamic light scattering (DLS), thioflavin T (ThT) assay, transmission electron microscopy (TEM), and atomic force microscopy (AFM) were used to explore the inhibition and disaggregation capability of oxidovanadium complexes against the fibrillization of hIAPP, hIAPP19–37, and hIAPP20–29. The binding interaction of oxidovanadium complexes with peptides was also studied using intrinsic fluorescence quenching and isothermal titration calorimetry (ITC). 3-(4,5-Dimethyl-2-thiazolyl)-2,5-diphenyl-2-H-tetrazolium bromide (MTT) assay, membrane leakage experiments, and immune assay were used to detect the cytotoxicity induced by hIAPP aggregation and the regulation of oxidovanadium complexes on cell viability and membrane protection.

2. Experimental section

2.1. Materials

The peptides hIAPP (KCNTATCATQRLANFLVHSSNNFGAILSSTNVGSNTY-NH_2), hIAPP19–37 (SSNNFGAILSSTNVGSNTY-NH_2), and hIAPP20–29 (SNNFG-AILSS-NH_2) were chemically synthesized and purified by Synpeptide Co., Ltd. (Shanghai, China). The peptides' purity was confirmed to be > 95% with HPLC-MS. Before use, the peptide was dissolved in hexafluoroisopropanol for 1 h to remove any preexisting aggregates and freeze dried at −55 °C for 12 h. The lyophilized peptides were dissolved in 10 mM phosphate buffer (PB, pH 7.4) and stored at −20 °C. Oxidovanadium complexes were prepared and identified using infrared (IR) and UV–visible (UV–vis) spectroscopy based on previous reports [47,48]. 1,2-Dioleoyl-sn-glycero-3-phosphocholine (DOPC, ≥99%) and 1,2-dioleoyl-sn-glycero-3-phospho-(1-rac-glycerol) (DOPG, ≥98%) were purchased from AVT Pharmaceutical Technology Co. Ltd. (Shanghai, China) and stored at −20 °C with nitrogen protection. Islet amyloid peptide anti-oligomer antibody A-11 [1000 times dilution in 0.01 M phosphate buffer saline (PBS, pH 7.4) with 1% bovine serum albumin (BSA)] was purchased from Shanghai Ulva Tries Biotechnology Co. Ltd. (Shanghai, China) and stored at −20 °C before use. All other reagents were of analytical grade.

2.2. UV spectrometry

The absorption peaks of three oxidovanadium complexes were identified using Cary 50 UV–vis spectrophotometer (Agilent Technologies Ltd., USA) at the scan range of 200–800 nm. The time-scale experiments of 20 μM oxidovanadium complex (5% dimethyl sulfoxide (DMSO)) in 10 mM PB (pH 7.4) were determined by UV–vis spectrometer at 0, 6, 12, and 24 h to evaluate the structural stability of these compounds. The UV spectra of 10 μM ThT in the presence of **1**, **2**, or **3** can be determined using spectrometer in 10 mM phosphate buffer (PB, pH 7.4). The prepared stock solution of oxidovanadium complexes was 100 μM in 5% DMSO aqueous solution. The final complex concentrations were 0, 2.5, 5, 7.5, 10, 15, and 20 μM. All data analyses were repeated in triplicate.

2.3. DLS analysis

Multimodal size distribution of hIAPP (10 μM), hIAPP19–37 (30 μM), and hIAPP20–29 (30 μM) aggregates were collected in the absence and presence of oxidovanadium complexes by using Nano-ZS90 Zetasizer Nano Series (Malvern Instruments Ltd., Worcestershire, UK). The molar ratios of the complex to the peptide were 5 and 10. For inhibition detection, the peptides were incubated with oxidovanadium complexes at 37 °C for 72 h in 10 mM PB (pH 7.4). The samples were

then centrifuged at 10,000 revolutions per minute (rpm) for 10 min to remove large particles. The supernatant fluid was used to determine the particle size. For disaggregation experiments, the oxidovanadium complexes were added after incubating the peptides at 37 °C for 72 h. The mixture was subsequently incubated at 37 °C for 72 h. The DLS data were acquired by the average of three results.

2.4. ThT assay

In the absence and presence of five fold excess of oxidovanadium complexes, hIAPP (10 μM), hIAPP19–37 (30 μM) and hIAPP20–29 (30 μM) in 10 mM PB (pH 7.4) were incubated at 37 °C for 72 h. After incubation, ThT was added at a final concentration of 20 μM. ThT fluorescence was examined using F-4600 fluorophotometer (Hitachi Ltd., Japan) with an excitation wavelength of 432 nm. The emission spectrum was acquired at a scan speed of 240 nm·min^{-1} and voltage of 700 V. The slit of excitation and emission was 10 nm. During disaggregation, hIAPP (10 μM), hIAPP19–37 (30 μM), and hIAPP20–29 (30 μM) in 10 mM PB (pH 7.4) were incubated at 37 °C for 72 h. Oxidovanadium complexes were subsequently added, and the samples were incubated for an additional 72 h at 37 °C. The final concentration of ThT was 20 μM. The time-scale experiments of peptide aggregation were performed in the absence and presence of **1**, **2**, and **3** at 484 nm for hIAPP, hIAPP19-37, and hIAPP20-29. The lag time was determined during the process as it represents the delay time of peptide nucleation [49]. After 72 h of incubation, IC_{50} value was derived from the 50% inhibitory rate of the three oxidovanadium complexes against hIAPP aggregation based on the ThT assay [50–52]. All reported data were derived from three experimental replicates.

2.5. TEM and AFM images

The samples of hIAPP (10 μM), hIAPP19–37 (30 μM), and hIAPP20–29 (30 μM) were prepared and incubated in the absence and presence of oxidovanadium complexes at 37 °C for 72 h. The molar ratios of the complex to the peptide were 5 and 10. For TEM morphology, an aliquot of the sample was spotted onto carbon-coated 600-mesh copper grids after co-incubation and stained with 2% phosphotungstic acid. Each aliquot occupied one grid individually. The specimens were air dried and viewed under a Hitachi H-800 electron microscope (Hitachi, Japan) at 200 kV. The final images were obtained from the average results of three experiments. For AFM analysis, the samples were incubated as mentioned above. Tapping mode was used at ambient temperature and standard conditions. Images were obtained on a silicon tip at a scanning rate of 1 Hz and a scanning line of 512 by using Bruker Nano Dimension Icon (Bruker Nano Inc., Germany).

2.6. Fluorescence determination

Intrinsic fluorescence quenching was conducted using F-4600 fluorophotometer (Hitachi Ltd., Japan) to observe oxidovanadium complex-induced solution conformational change of hIAPP and its fragments [53]. The peptide concentrations measured 10, 30, and 30 μM for hIAPP, hIAPP19–37, and hIAPP20–29, respectively. Different oxidovanadium complexes were appended into the peptide solution within a 0–8 M ratio for the three peptides. For hIAPP and hIAPP19–37, the tyrosine (Tyr) residue Tyr37 was excited at 275 nm. For hIAPP20–29, the phenylalanine (Phe) residue Phe23 was excited at 260 nm. The experiments were repeated in triplicate.

2.7. ITC study

The thermodynamic parameters of peptides binding to oxidovanadium complexes were determined using MicroCal ITC200 (Malvern Instruments Ltd., UK) at 25 °C. **1** was dissolved in a 10 mM PB (pH 7.4), **2** and **3** were dissolved in a 10 mM PB (5% DMSO, pH 7.4). All solutions were degassed prior to use through a 0.22 μM filter membrane and adjusted to pH 7.4. The final concentration of the peptides ranged from 10 μM to 20 μM. Titration of oxidovanadium complexes into the peptides can be obtained after subtracting the background. The reference sample was the mentioned buffer titrated by the complexes. Injections were conducted 10 min apart to maintain the thermal equilibrium. An initial injection of 0.5 μL of the complex was followed by 14 additional injections of 2.5 μL of the complexes into the peptide. The stirring rate was 1000 rpm. The oxidovanadium complex was sucked into the syringe with an initial concentration of 400–1500 μM of each compound. The experiments were performed in triplicate.

2.8. MTT assay

Cytotoxicity induced by peptides was tested following the standard MTT method. The rat insulinoma (INS-1) line was obtained from Bogoo Biotech Co., Ltd. (Shanghai, China). The cells were cultured in 1640 (Gibco) culture medium with 10% fetal bovine serum, incubated at 37 °C in a humidified 5% CO_2 incubator (Sanyo, MCO-15 AC, Japan) for 24 h, and further incubated with 15 μM hIAPP, hIAPP19–37, or hIAPP20–29 (pH 7.4) for 72 h in the absence and presence of oxidovanadium complexes. The final concentration of each oxidovanadium complex was set to 15 μM, and 10 μL of 5 mg/mL MTT was added into each well. The plate was incubated at 37 °C for 4 h [54]. Cell survival was assessed by checking the MTT reduction. The medium was carefully removed, and each well was added with 200 μL of DMSO. The average absorption value at 490 nm was reported after performing the experiments four times. One-way analysis of variance with post hoc Dunnett's test produced the adopted results. A level of $p < 0.05$ was determined as significant.

2.9. Membrane leakage experiments

In brief, 10 mM lipidosome consisting of DOPC and DOPG (7:3) was dissolved in 1 mM calcein buffered by 10 mM PB (pH 7.4) by ultrasound mixing. Size-exclusion column chromatography (Sephadex G-50 fine) was used to remove free calcein from the calcein-filled lipidosome by eluting with 10 mM PB (pH 7.4). The diluted solution contained 30 μM peptide, 5 μM calcein, and 100 μM liposomes. The fluorescence of calcein was recorded every 60 min from 0 to 15 h. Membrane leakage induced by peptide aggregation was detected in the presence of oxidovanadium complexes. The molar ratio of the complex to the peptide was 5. The peptide alone was measured as a control. After each assay, 1 μL of 10% Triton X-100 was added to assess the maximum membrane leakage. Membrane leakage assay was obtained according to the equation [12]:

$$L(t) = (F_t - F_0)/(F_{100} - F_0)$$

where L(t) is the normalized membrane leakage, and F_t is the fluorescence intensity at each time. F_0 and F_{100} are the fluorescence intensities at $t = 0$ and after addition of Triton X-100, respectively. The results were the average of three experiments.

2.10. Immune assay

Standard enzyme linked immunosorbent assay (ELISA) was conducted to explore the oligomers by binding to the A-11 antibody [55]. The peptide sample in the absence and presence of oxidovanadium complex was spotted on 96-well plates after incubating in the dark at 25 °C for 12 h. In brief, 10 μL of the A-11 antibody in 1000 times dilution with 1% BSA was used and buffered by 0.05 M carbonate solution (pH 9.6) at 4 °C for 12 h. The concentrations of the peptide and oxidovanadium complex were 30 μM. The plates were washed by 0.01 M phosphate buffer saline-0.001% Tween 20 (PBST) three times at pH 7.4, sealed with 2% BSA, and incubated at 37 °C for 2 h. Goat anti-rabbit antibody was diluted 10,000 times with 1% BSA before use. The

final samples were obtained following the standard plate washing program and treated with 3,3',5,5' tetramethyl benzidine (TMB) coloration kit at 25 °C for 8 min to record OD values at 450 nm. Data distribution and analysis methods were described as in MTT assay. The experiments were repeated four times, and the results were averaged.

3. Results and discussion

3.1. Synthesis of oxidovanadium complexes

The three oxidovanadium complexes (**1**, **2**, and **3**) were synthesized and identified with yields of 40%, 80%, and 42% respectively. Figs. S1 and S2 show the UV/vis and IR spectra of the oxidovanadium complexes, and the results are consistent with those of other studies [47,48,56–59]. The IR results (KBr disk, cm^{-1}) were $\nu_{V=O}$ = 945 cm^{-1} (**1**), $\nu_{V=O}$ = 993 cm^{-1} (**2**), and $\nu_{V=O}$ = 945 cm^{-1} (**3**). The UV/vis results (20 μM, 5% DMSO in 10 mM PB (pH 7.4)) were λ_{max} = 281 nm (**1**), λ_{max} = 275 nm (**2**), and λ_{max} = 281 nm (**3**). According to the molecular formulas of **1** ($C_{10}H_{20}N_3O_9V$), **2** ($C_{14}H_{14}O_7V$), and **3** ($C_{30}H_{38}N_6O_{12}V_2$), the obtained elemental analysis results were consistent with the calculated values within an error range of 0.5% (Table S1). Fig. S3 shows the time-scale spectra of 20 μM oxidovanadium complexes **1**, **2**, and **3**. The absorption peaks of the compounds had slight change with time. Based on previous pH-dependent V^{51} NMR and ESR reports, the species were $[VO(O_2)_2\mathbf{L}]\cdot H_2O$, $[VO(O_2)_2\mathbf{L}]^-$, $[VO(O_2)_2(H_2O)\mathbf{L}]\cdot H_2O$, $[VO(O_2)_2(NH_3)]$ in **1**, $[VO\mathbf{L}_2]$, $[(VO)_2\mathbf{L}_2(OH)_2]$, $[(VO)_2(OH)_5]^-$, $[VO\mathbf{L}_2(OH)]^-$ in **2**, and $[O\{VO(\mathbf{L})\}_2]$, $[(VO\mathbf{L})_2(OH)_2]$ in **3**. The major species were $[VO(O_2)_2\mathbf{L}]\cdot H_2O$ and $[O\{VO(\mathbf{L})\}_2]$ for **1** and **3** respectively [56,57,59,60]. $[VO\mathbf{L}_2]$ accounted for the highest proportion in **2**, after comparing with previous work [58]. A probable mechanism of **2** in solution is depicted in Scheme S1.

3.2. Inhibition by oxidovanadium complexes in peptide aggregation

DLS analysis was performed to gain insights into the particle size distribution of amyloid peptides and the influence of oxidovanadium complexes. Fig. 1 shows the multimodal size distribution of hIAPP (10 μM), hIAPP19–37 (30 μM), and hIAPP20–29 (30 μM) in the absence and presence of **1**, **2**, and **3**. After incubation, the maximum particle size distribution increased to approximately 5400 nm for hIAPP and hIAPP19–37. In contrast to previously studied hIAPP30–37 and hIAPP1–19, the short peptide hIAPP20–29 presented the maximum distribution at 900 nm owing to the difficulty of forming a core of aggregation and producing numerous fibrils [44,61]. The aggregation of hIAPP and its fragments reduced with increasing oxidovanadium complexes. Table S2 demonstrates the particle size of peptide aggregates in the presence of oxidovanadium complexes obtained by DLS analysis. The aggregate size by oxidovanadium complexes ranged from the microscale to the nanoscale, and the best inhibitory effect of oxidovanadium complexes was against full-length hIAPP. The complexes showed a relative indistinctive effect on hIAPP20–29. Among the complexes, **3** displayed the strongest inhibitory effect against peptide aggregation.

The results of the ThT assay indicated that the peptides aggregated based on the increasing ThT fluorescence intensity (Fig. 2). The fluorescence intensity notably decreased upon the addition of **1**, **2**, or **3**. The inhibitory effect of **2** and **3** was stronger than that of **1** for hIAPP and hIAPP19–37, consistent with the DLS results. By contrast, the influence of the three complexes on hIAPP20–29 aggregation was weaker than that on the other two peptides. Furthermore, the dynamic experiments indicated different lag times, indicative of the inhibition of metal complexes against peptide aggregation (Table 1), consistent with the observation of ThT assay. With increasing oxidovanadium complexes, the lag time prolonged. These compounds showed an antifibrillogenic activity with elongation of the nucleation phase and decrease in the aggregation extent. For **3**, the longest lag time implied strong inhibition against peptide aggregation.

UV spectroscopy analysis was performed to clarify the possible interaction of ThT with oxidovanadium complexes, and the resulting spectra are shown in Fig. S4. With the addition of the complexes, their characteristic peak increased, but that of ThT at 412 nm remained unchanged. The oxidovanadium complexes underwent no notable interaction with ThT. Therefore, the ThT assay may effectively demonstrate the extent of peptide aggregation and the influence of oxidovanadium complexes on hIAPP and its fragments.

Through concentration-dependent experiments using ThT assay, we calculated the IC_{50} values to compare the inhibition capabilities of the complexes with peptide aggregation. IC_{50} is defined as the inhibitor concentration when achieving 50% of the maximum effects on peptide aggregation [18]. The IC_{50} values of the three complexes are shown in Table 1. The values were found to be within the micromolar range, suggesting their strong inhibitory effect against hIAPP aggregation, consistent with DLS results. Complex **3** showed the most significant inhibition, as indicated by its IC_{50} values of 8.5 and 39.6 μM against hIAPP and hIAPP19–37, respectively. Compared with a previous study, BEOV (**2**) yielded an IC_{50} value similar to that of BMOV against hIAPP [32], and **3** featured a lower IC_{50} value against hIAPP than against PrP106–126 [15].

The analysis of particle size distribution and ThT fluorescence intensity revealed the different aggregation capabilities of the three peptides in the following order, hIAPP > hIAPP19–37 > hIAPP20–29. hIAPP20–29 is a fragment of the hIAPP core region, and the whole length of peptide hIAPP1–37 highly self-aggregates to form amyloid fibrils. The three oxidovanadium complexes significantly affected peptide aggregation, and **3**, which had the largest aromatic molecular configuration, displayed the strongest inhibitory effects on peptide amyloidosis. Compared with previous works, **3** showed better inhibition on hIAPP than on prion neuropeptide.

3.3. Morphological analysis of three peptides

The TEM and AFM images indicated that peptide fibril formation was effectively inhibited by the oxidovanadium complexes (Figs. 3 and S5). The TEM images showed that self-assembly of hIAPP and hIAPP19–37 produced distinct winding fibrils after incubation for 72 h at 37 °C [32,62]. The aggregation capability of hIAPP19–37 was stronger than that of short fragment hIAPP20–29 to form mature fibrils (Fig. 3). With increasing oxidovanadium complexes to 5- and 10-fold excess, the fibrils of hIAPP and hIAPP19–37 gradually decreased and formed globular oligomers and monomers. The fragment of hIAPP20–29 failed to form numerous fibrils but formed oligomers after incubation. The addition of the oxidovanadium complexes decreased hIAPP20–29 aggregates, and the oligomers were further reduced.

The AFM images were similar to those of the TEM images (Fig. S5), indicating inhibition of peptide fibril formation by the oxidovanadium complexes studied. The concentration dependence of the oxidovanadium complexes was observed with morphological changes in the hIAPP and hIAPP19–37 aggregates. Table S3 shows the heights of peptide aggregates along with the lines in Fig. S4. A mature amyloid fibril typically stretches to approximately 9 nm for cross-sectional height [63]. With increasing oxidovanadium complexes, the aggregate shape was altered from fibrils to spherical and amorphous particles. Hence, the height of the peptide aggregates first increased and then decreased, similar to previous observations [63]. The results of TEM and AFM morphological analyses are consistent with those of ThT assay and DLS analysis.

Morphological observation elucidated that oxidovanadium complexes reversed peptide fibril formation. Based on the AFM images and the results of the ThT assay, BEOV elicited similar inhibitory effect against hIAPP to that against BMOV [31], suggesting that a long carbon skeleton may not be the major factor affecting inhibition. Moreover, **3** showed better inhibitory effect against hIAPP than against PrP106–126 because considerable fibrils appeared under the same condition [15].

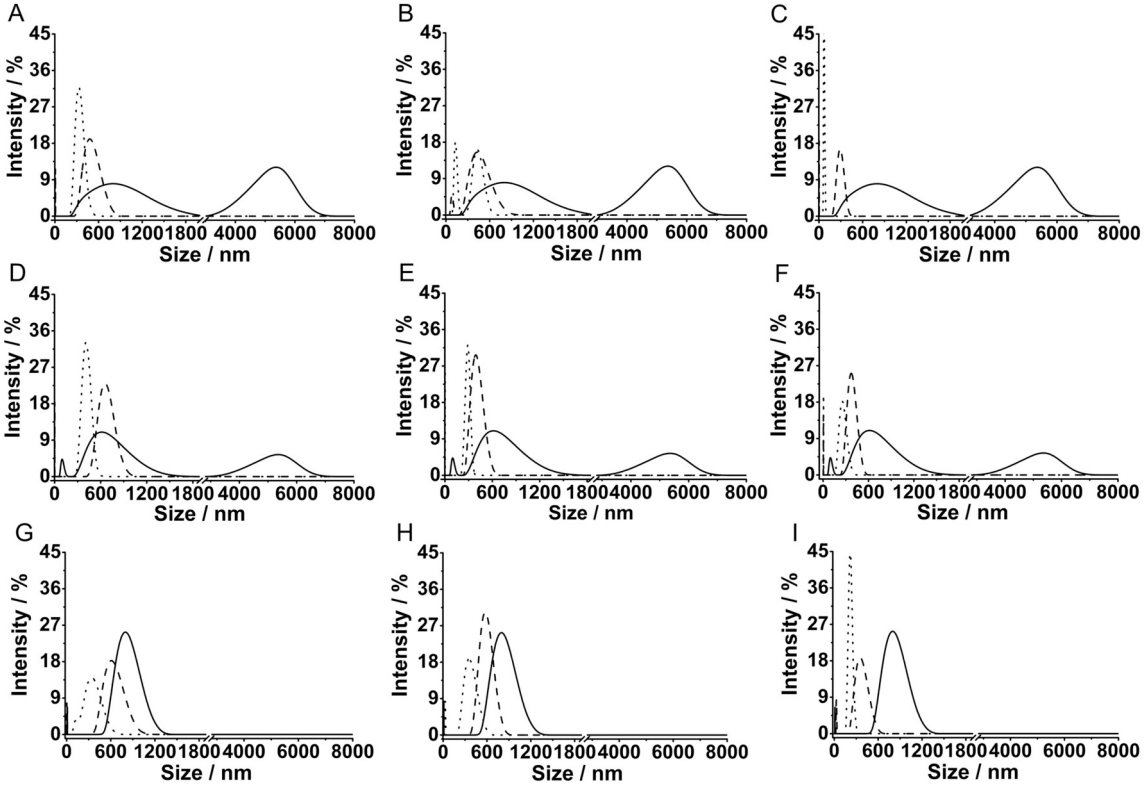

Fig. 1. DLS analysis of the multimodal size distribution of 10 μM hIAPP (A–C), 30 μM hIAPP19-37 (D–F), and 30 μM hIAPP20-29 (G–I) aggregates in the absence (solid) and presence of 5 (dashed) and 10 fold excess (dotted) of **1** (A, D, G), **2** (B, E, H) and **3** (C, F, I).

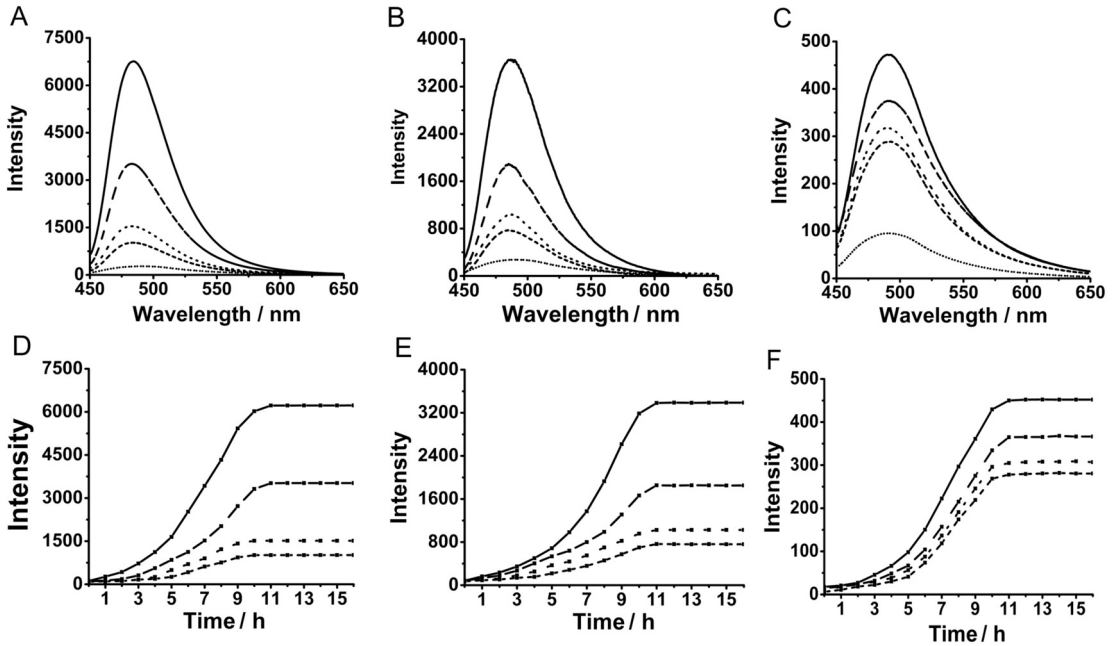

Fig. 2. ThT assay for the peptides hIAPP, hIAPP19-37, and hIAPP20-29 aggregation in the absence (solid) and presence of five fold excess of **1** (dashed), **2** (dotted), and **3** (short dashed). ThT (short dotted) was used as a marker. The concentration of peptide was 10 μM, 30 μM, and 30 μM, respectively. Fluorescent kinetics of peptides aggregation in the absence (solid) and presence of five fold excess of **1** (dashed), **2** (dotted), and **3** (short dashed) at 484 nm for hIAPP (D), hIAPP19–37 (E), and hIAPP20–29 (F).

3.4. Changes in peptide conformation by oxidovanadium complexes

To elucidate the interaction between hIAPP and current oxidovanadium complexes and the effects of these compounds on peptide conformation, we carried out experiments on intrinsic fluorescence quenching. Different residues were used for different peptides because hIAPP and hIAPP19–37 contain the aromatic residue Tyr37 and hIAPP20–29 contains residue Phe23. With the addition of the oxidovanadium complexes, peptide fluorescence was quenched and the peak intensity gradually decreased (Fig. S6). The fluorescence quenching of

Table 1
IC_{50}[a] values and lag time[b] for the inhibition of oxidovanadium complexes against peptide fibrils aggregation (pH 7.4).

Complexes	hIAPP		hIAPP19-37		hIAPP20-29	
	IC_{50}	Lag time/h	IC_{50}	Lag time/h	IC_{50}	Lag time/h
0	–	1.5	–	1.5	–	1.0
1	33.0 ± 1.1	3.0	71.9 ± 2.5	2.0	76.4 ± 2.7	1.5
2	14.7 ± 0.6	4.0	51.2 ± 1.1	3.0	69.5 ± 2.3	2.5
3	8.5 ± 0.5	4.5	39.6 ± 1.0	4.0	62.3 ± 2.0	3.0

[a,b]Values were measured by the ThT and fluorescent kinetics assay.

the aromatic residues implied the alteration in the peptide conformation due to binding to oxidovanadium complexes. Given this molecular structure feature, we assume that the aromatic group in the oxidovanadium complexes may contribute to the interaction and inhibition of metal complexes against hIAPP and its fragments, as reflected by other inhibitors, such as epigallocatechin gallate and the possible existence of π-stacking [65].

3.5. Determining the thermodynamic behavior of peptides with oxidovanadium complexes by ITC

ITC has been widely applied in the biomedical field, such as in studies on antigen–antibody, cell metabolism, enzyme inhibitors, and DNA–drug interaction [66]. The studied reactions produced the bound

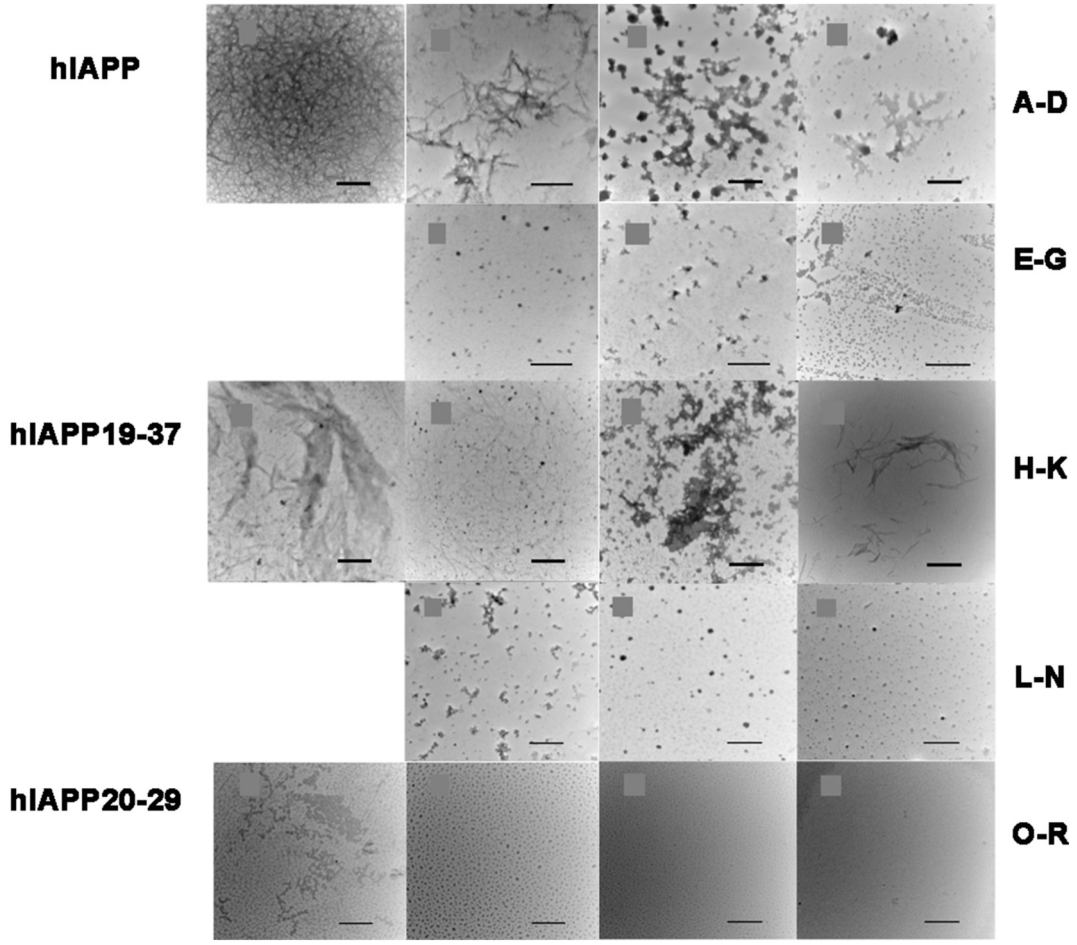

Fig. 3. TEM images of 10 μM hIAPP (A), 30 μM hIAPP19-37 (H), and 30 μM hIAPP20-29 (O) in the absence and presence of 5 (B–D, I–K, P–R) and 10 fold excess (E–G, L–N) of **1** (B, E, I, L, P), **2** (C, F, J, M, Q) and **3** (D, G, K, N, R), respectively. The scale bar is 500 nm in TEM. The labels are sorted from left to right.

Table 2
Thermodynamic parameters of oxidovanadium complexes binding to hIAPP, hIAPP19-37, and hIAPP20-29 at 25 °C.

Complexes	ΔG^0 (kJ·mol^{-1})	ΔH^0 (kJ·mol^{-1})	ΔS^0 (J·mol^{-1}·K^{-1})	K_d ($\times 10^{-6}$ M)
hIAPP + **1**	−25.63 ± 0.04	−5.81 ± 0.08	66.51 ± 0.13	32.15 ± 1.18
hIAPP + **2**	−18.57 ± 0.12	−29.30 ± 0.03	−36.01 ± 0.30	555.50 ± 70.0
hIAPP + **3**	−26.73 ± 0.05	3.20 ± 0.10	100.44 ± 0.50	20.66 ± 0.97
hIAPP19-37 + **1**	−23.39 ± 0.08	0.67 ± 0.09	80.74 ± 0.57	79.42 ± 5.29
hIAPP19-37 + **2**	−21.29 ± 0.12	4.54 ± 0.18	86.68 ± 1.01	185.20 ± 23.13
hIAPP19-37 + **3**	−17.35 ± 0.10	10.83 ± 0.19	94.56 ± 0.97	909.10 ± 76.10
hIAPP20-29 + **1**	−24.57 ± 0.05	3.34 ± 0.01	93.66 ± 0.21	49.31 ± 2.51
hIAPP20-29 + **2**	−26.47 ± 0.03	−34.98 ± 0.20	−28.56 ± 0.57	22.93 ± 0.63
hIAPP20-29 + **3**	−17.35 ± 0.29	17.64 ± 0.37	117.42 ± 0.27	909.11 ± 73.22

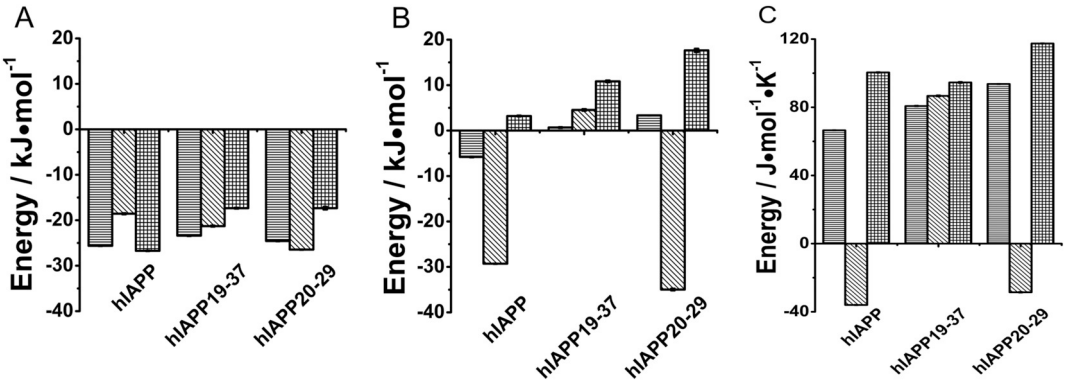

Fig. 4. The binding thermodynamic parameters of hIAPP, hIAPP19-37, and hIAPP20-29 with complexes **1** (transverse), **2** (right slash), and **3** (square) respectively. The histograms represent ΔG^0 (A), ΔH^0 (B), and ΔS^0 (C) obtained at 25 °C.

species due to the interactions of oxidovanadium complexes and peptides accompanying with the heat change. Fig. S7 displays the thermal determination of peptides binding to oxidovanadium complexes at 25 °C. The heat flow gradually reached the equilibrium with the titration of oxidovanadium complexes. Table 2 shows the thermodynamic parameters of the complexes bound to the three peptides. Data were obtained after subtracting the background of the titration buffer. The negative binding Gibbs free-energy change (ΔG^0) suggests spontaneous interaction. Based on the results of K_d, the oxidovanadium complexes showed a relatively similar binding affinity to hIAPP and its fragments. Fig. 4 illustrates the difference in thermodynamic behavior between the complexes and the three peptides. A distinct binding enthalpy change (ΔH^0) was observed for different complexes and peptides. Comparison of ΔH^0 and the entropy change (ΔS^0) of the reaction system identified a notable entropy-driven process for the binding of **1** and **3** to hIAPP and hIAPP19–37, respectively; the hydrophobic interaction was supposed to be a primary driving force for hIAPP with complexes [67,68]. Meanwhile, the binding of **2** to hIAPP or hIAPP20–29 showed an enthalpy-

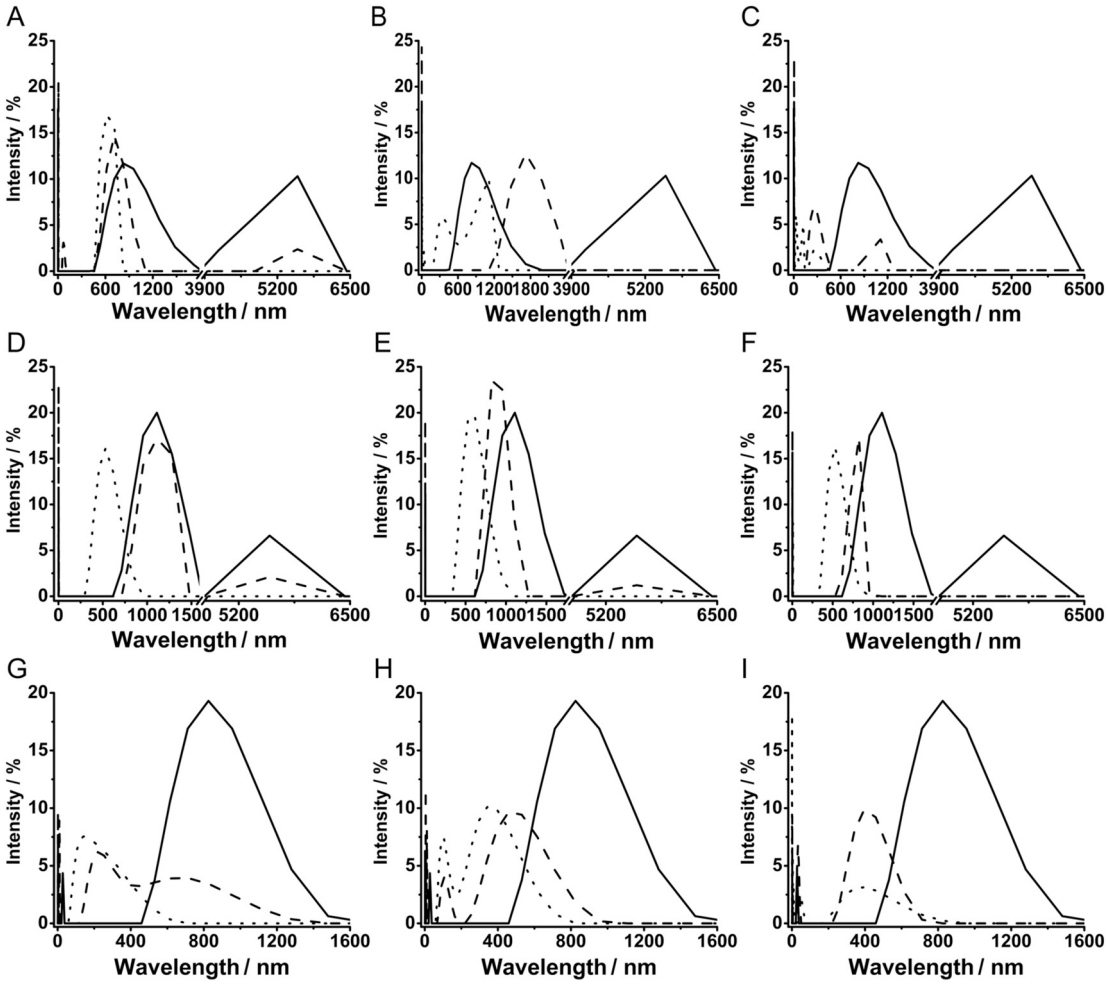

Fig. 5. DLS analysis of the multimodal size distribution of 10 μM hIAPP (A–C), 30 μM hIAPP19-37 (D–F), and 30 μM hIAPP 20-29 (G–I) fibril disaggregation in the absence (solid) and presence of 5 (dashed), and 10 fold excess (dotted) of **1** (A, D, G), **2** (B, E, H), and **3** (C, F, I).

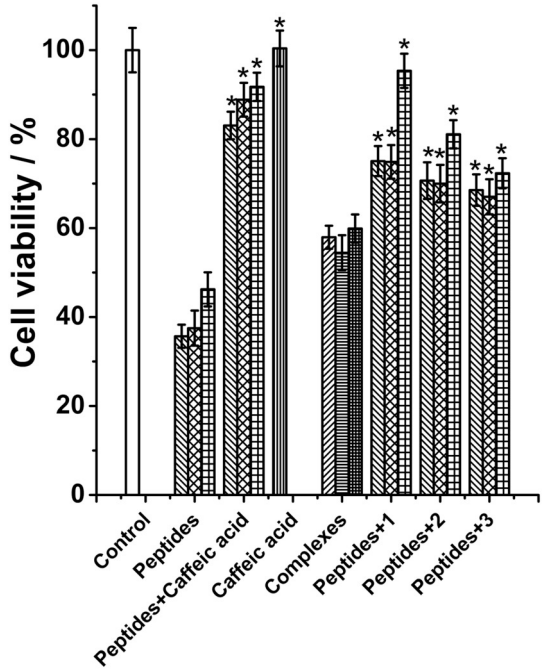

Fig. 6. INS-1 cells viability determined by MTT assay. The cells were treated with the peptide hIAPP (right slash), hIAPP19-37 (diagonal grid), and hIAPP20-29 (square) (15 μM, pH 7.4), or treated with peptides and 15 μM **1**, **2** and **3**, respectively. 15 μM caffeic acid was used as negative control (long string). INS-1 cells were treated with 15 μM **1** (left slash), **2** (transverse), and **3** (thick square), respectively. The control was in white. Data are shown as means ± SD, n = 3. **p < 0.05 compared to the negative control of peptide by one-way ANOVA.

driven process, and this condition could possibly involve favorable cation–π interaction [67].

This work revealed that oxidovanadium complexes bound to hIAPP and its fragments through hydrophobic and other molecular interactions. Our previous studies revealed that redox oxidovanadium complexes, such as **1**, inhibit the aggregation of prion neuropeptide PrP106–126 and amyloid β (Aβ) through methionine oxidation [18]. The absence of methionine in hIAPP results in different interaction mechanisms between hIAPP and these oxidovanadium complexes [31,32]. In addition to hIAPP-associated T2DM, amyloid fibril formation is linked to various neurodegenerative diseases, such as Aβ in Alzheimer's disease (AD), αS in Parkinson's disease, and PrP in prion disorder [69–72]. Patients with T2DM often manifest AD symptoms, particularly amyloidosis [73–75]. Comparison of hIAPP and Aβ binding to vanadium complexes demonstrated that the vanadium complexes acted well on different amyloid peptides despite their notably different interaction mechanisms.

3.6. Peptide disaggregation affected by oxidovanadium complexes

Disaggregation experiments may reveal the capability of oxidovanadium complexes to interrupt the formation of fibrils. Fig. 5 shows the DLS particle size distribution of the peptide aggregates. The oxidovanadium complexes can effectively scatter the mature aggregates. Compared with the inhibition results shown in Fig. 1, the particle size was > 1000 nm for hIAPP when the molar ratio was 5. The results were considered reasonable because the peptide molecules mutually bound to form mature fibrils, and the interaction between complexes and peptide molecules was more difficult than with hIAPP alone. Fig. S8 indicates that the three peptides were disaggregated by the oxidovanadium complexes based on the results of the ThT fluorescence assay. The fluorescence intensity decreased gradually with the addition of the metal complexes. The disaggregation capability of **1** against hIAPP fibrillation was weaker than that of **2** and **3**. However, the effects of these complexes on hIAPP20–29 were similar to that of **1** because the short peptide experienced difficulty in forming mature fibrils [61]. Hence, the three complexes showed no remarkable differences.

The oxidovanadium complexes showed remarkable disaggregation capability against fibrosis of different hIAPP fragments. With increasing number of benzene rings, the inhibition and disaggregation capabilities of these small molecules increased. The disaggregation capabilities of **2** and **3** were superior to that of **1** against hIAPP, hIAPP19–37, and hIAPP20–29 aggregation. Vanadium binds to two bipyridyl groups in **3**, and **2** contains bis(ethyl-maltolato, *O*,*O*) ligands, which may feature increased space resistance to interrupt the formed fibrils. As shown in Scheme S1, the hydration of [VO**L**$_2$] produced the species of cis-[VO**L**$_2$(H_2O)] which may be primarily responsible for the current biological effects [58].

This work employed three peptides to compare aggregation behavior. Shortening the length of the peptide sequence reduced the capability for peptide aggregation, and the disaggregation capability of the three oxidovanadium complexes was not distinguished. By comparing the interactions of existent inhibitors with those of hIAPP [12,65], we speculate that the H-bonds of peptide aggregates were broken, and hydrophobic interaction, van de Waals force, and π–π stacking contributed to the binding of the oxidovanadium complexes to hIAPP.

3.7. Cell viability, membrane protection, and immunodetection

Amylin is one of the peptides that aggregate spontaneously and cause β-cell apoptosis, which is related to T2DM [76]. The misfolding and self-aggregation of hIAPP are key factors of the cytotoxicity of INS-1 cells in rats. In this work, INS-1 cells were used to evaluate the effects of the oxidovanadium complexes on cytotoxicity involved in T2DM pathogenesis [64]. Fig. 6 displays the viability of INS-1 cells alone and under treatment with peptides in the absence and presence of the oxidovanadium complexes. The obtained data obeyed a normal distribution according to the statistical analysis (SPSS 17.0) [77]. The viability of the cells treated with peptide alone reached 35.7% ± 2.6%, 37.5% ± 3.2%, and 46.2% ± 3.8% for hIAPP, hIAPP19–37, and hIAPP20–29, respectively. In the presence of the three oxidovanadium complexes, cytotoxicity in INS-1 cells induced by hIAPP and hIAPP20–29 decreased, and a significant difference was also observed compared with the positive control of the peptide itself. By contrast, the complexes may prominently alleviate the cytotoxicity induced by hIAPP20–29 than that induced by hIAPP19–37. The clinically studied BEOV (**2**) presented desirable effects on reducing cytotoxicity, which is comparable with that of BMOV [31].

After our parallel cytotoxicity experiments using oxidovanadium complexes alone, we found that the effects of the oxidovanadium complexes on INS-1 cells to a certain extent. However, the co-incubation of the metal complexes with the peptides could significantly reverse the toxicity of INS-1 cells. Given the self-toxicity of the oxidovanadium complexes, they appeared to be not within a reasonable therapeutic window. Vanadium complexes may also interact with other targets, such as DNA and specific enzymes in cells [33,34]. Further studies should be conducted to elucidate the mechanisms of this phenomenon, and in-depth structural refinement of oxidovanadium complexes must be conducted to improve their medical properties.

Peptide-caused membrane leakage was explored in the presence of the oxidovanadium complexes. Amyloid oligomers and fibrils formed gradually and abundantly with time, causing the membrane disruption and diosmosis and killing the cells ultimately [12]. The addition of the oxidovanadium complexes decreased the membrane leakage (Fig. 7). The results are consistent with the peptide growth phases as observed in the ThT kinetics assay (Fig. 2), indicating the inhibition of the oxidovanadium complexes against peptide aggregation.

ELISA of the A-11 antibody was conducted in the absence and presence of oxidovanadium complexes to clarify if the oxidovanadium

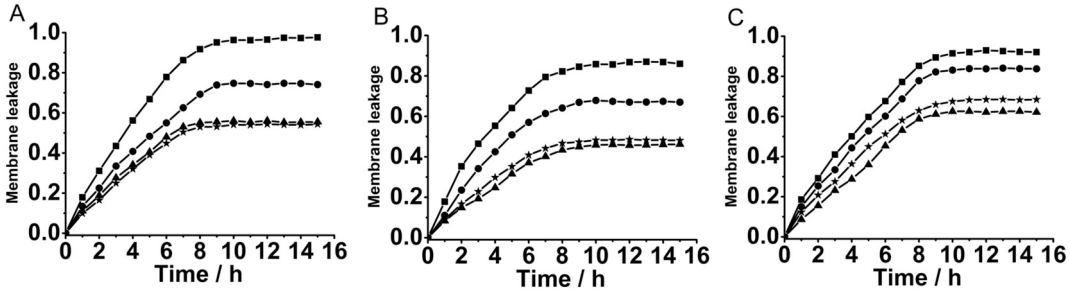

Fig. 7. Normalized membrane leakage of 30 μM hIAPP (A), hIAPP19-37 (B), and hIAPP20-29 (C) in the absence (square) and presence of 5 fold excess of **1** (round), **2** (triangle), and **3** (starlike). Calcein and liposomes were 5 μM, 100 μM in solution respectively.

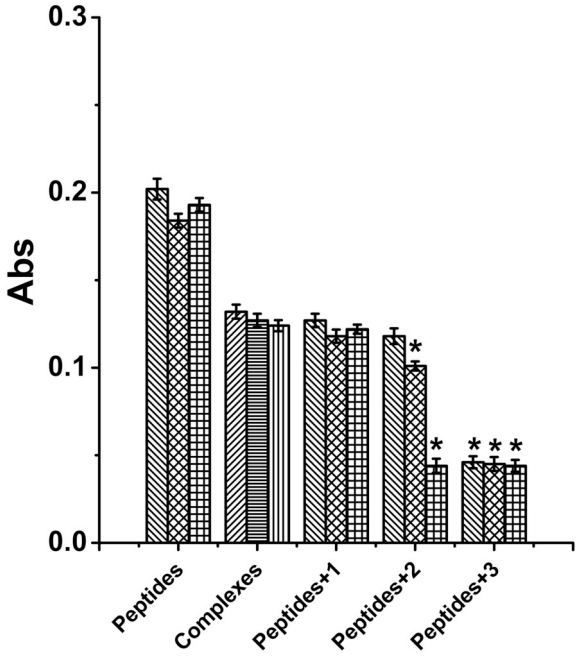

Fig. 8. ELISA assay of A-11 antibody with the peptides hIAPP (right slash), hIAPP19-37 (diagonal grid), and hIAPP20-29 (square) (30 μM) oligomers in the absence and presence of 30 μM **1**, **2** and **3**, respectively. The A-11 antibody was treated with the 30 μM **1** (left slash), **2** (transverse), and **3** (long string). Data are shown as means ± SD, n = 3 in normal distribution. **p < 0.05 compared to the peptide oligomers by one-way ANOVA.

complexes inhibit the formation of peptide oligomers [55]. A-11 antibody is used to bind and stain toxic oligomers [78]. Differences between peptide oligomers with or without oxidovanadium complexes are shown in Fig. 8. The absorption intensity decreased in the presence of the oxidovanadium complexes. The remarkable intensity change in **3** revealed that the decline in peptide oligomerization inhibited by the oxidovanadium complex, thereby weakening the binding of the peptide oligomers with the A-11 antibody.

Oxidovanadium complexes may play a critical role in reversing the dysfunction and apoptosis of β-cells induced by peptide fibril formation because they effectively disaggregate the formed fibrils and reduce the cytotoxicity caused by peptide aggregation. Oligomers play a more important role in peptide-induced cytotoxicity than fibrils. Morphological analysis showed that oligomers may still exist after incubation with the oxidovanadium complexes, but the appearance of numerous unobservable monomers could be the major source of the improvement of the viability of INS-1 cells [64]. Moreover, the immune assay of the A-11 antibody elucidated that oligomers were reduced after the peptides were incubated with the oxidovanadium complexes. These oxidovanadium complexes could reduce the formation of toxic oligomers, prevent the cytomembrane from penetrating, and upregulate the cell viability.

4. Conclusion

Applications of oxidovanadium complexes have been sustainably developed in the biomedical field. The three oxidovanadium complexes employed in the current work showed strong inhibitory effects, desirable disaggregation capability, and significant regulatory effect on cytotoxicity induced by amyloidosis of hIAPP and its fragments. Inhibition and disaggregation of amyloid peptide fibrils are vital to treatment of T2DM. The inhibition of the oxidovanadium complexes against hIAPP fibril formation was stronger than that against hIAPP19–37 and hIAPP20–29. Different ligand configurations, steric hindrance, ligand quantity, and coordination mode of vanadium ions may play a key role in the binding affinity and inhibition of peptide aggregation. Thermodynamic studies indicated that the oxidovanadium complexes bind to these peptides through hydrophobic and other molecular interactions with various binding thermal behavior and entropy change characteristics. Complexes **2** and **3** significantly disaggregated hIAPP and hIAPP19–37 fibrils and rescued peptide-induced cytotoxicity, whereas their capability to reverse the worse condition fibrillated hIAPP20–29 resembled that of **1**. Among the three compounds, **3** showed the highest potential to be used as hIAPP inhibitor. Oxidovanadium complexes are a series of potential candidates for treating amyloidosis, and further work should be performed to refine their configuration, decrease their self-cytotoxicity, and reveal their roles in protein and peptide-related conformational disorders.

Abbreviations

hIAPP	human islet amyloid polypeptide
T2DM	type II diabetes mellitus
bipy	2,2' bipyridine
BMOV	bis(maltolato) oxovanadium
BEOV	bis(ethyl-maltolato, *O*,*O*) oxidovanadium(IV)
PrP	prion protein
DLS	dynamic light scattering
ThT	thioflavin T
TEM	transmission electron microscopy
AFM	atomic force microscopy
ITC	isothermal titration calorimetry
MTT	3-(4,5-dimethyl-2-thiazolyl)-2,5-diphenyl-2-H-tetrazolium bromide
PBS	phosphate buffer saline
PB	phosphate buffer
IR	infrared
UV–vis	ultraviolet-visible
DOPC	1,2-Dioleoyl-sn-glycero-3-phosphocholine
DOPG	1,2-dioleoyl-sn-glycero-3-phospho-(1-rac-glycerol)
Tyr	tyrosine
Phe	phenylalanine

Aβ	amyloid-β
rpm	revolution per minute
INS-1 cells	insulinoma β-cells in rat
ELISA	enzyme linked immunosorbent assay
PBST	phosphate buffer saline-0.001% Tween 20
TMB	3,3',5,5' tetramethyl benzidine
SPSS	statistical package for the social sciences
ANOVA	analysis of variance

Acknowledgements

The project is supported by the National Natural Science Foundation of China (Nos. 21473251 & 21271185).

Appendix A. Supplementary data

Supplementary data to this article can be found online at https://doi.org/10.1016/j.jinorgbio.2019.110721.

References

[1] D.L. Hay, S. Chen, T.A. Lutz, D.G. Parkes, J.D. Roth, Pharmacol. Rev. 67 (2015) 564–600.
[2] P. Westermark, C. Wernstedt, E. Wilander, D.W. Hayden, T.D. O'Brien, K.H. Johnson, Proc. Natl. Acad. Sci. U. S. A. 84 (1987) 3881–3885.
[3] G. Vardatsikos, M.Z. Mehdi, A.K. Srivastava, Int. J. Mol. Med. 24 (2009) 303–309.
[4] R.A. Defronzo, Diabetes 58 (2009) 773–795.
[5] J.W. Kim, J.R. Kim, S.J. Yi, K.H. Shin, H.S. Shin, S.H. Yoon, J.Y. Cho, D.H. Kim, S.G. Shin, I.J. Jang, Clin. Ther. 33 (2011) 1819–1830.
[6] C.J. Bailey, A.A. Tahrani, A.H. Barnett, Lancet Diabetes Endocrinol. 4 (2016) 350–360.
[7] P. Krotee, J.A. Rodriguez, M.R. Sawaya, D. Cascio, F.E. Reyes, D. Shi, J. Hattne, B.L. Nannenga, M.E. Oskarsson, S. Philipp, Elife 6 (2017) 19273–19299.
[8] D.C.R. Camargo, K. Tripsianes, K. Buday, A. Franko, C. Gobl, C. Hartlmuller, R. Sarkar, M. Aichler, G. Mettenleiter, M. Schulz, Sci. Rep. 7 (2017) 44041–44052.
[9] M. Tatareknossol, L.M. Yan, A. Schmauder, K. Tenidis, G. Westermark, A. Kapurniotu, Chem. Biol. 12 (2005) 797–809.
[10] A.V. Kristen, S. Lehrke, S. Buss, D. Mereles, H. Steen, P. Ehlermann, S. Hardt, E. Giannitsis, R. Schreiner, U. Haberkorn, Clin. Res. Cardiol. 101 (2012) 805–813.
[11] P. Velander, L. Wu, W.K. Ray, R.F. Helm, B. Xu, Biochemistry 55 (2016) 4255–4258.
[12] B. Ren, Y. Liu, Y. Zhang, Y. Cai, X. Gong, Y. Chang, L. Xu, J. Zheng, ACS Chem. Neurosci. 9 (2018) 1215–1224.
[13] I. Zawisza, M. Rozga, W. Bal, Coord. Chem. Rev. 256 (2012) 2297–2307.
[14] D.C. Crans, Cheminform 80 (2015) 11899–11935.
[15] B. Zhang, D. Zhu, W. Wang, G. Gong, W. Du, RSC Adv. 6 (2016) 17083–17091.
[16] T. Scior, J.A. Guevara-Garcia, F.J. Melendez, H.H. Abdallah, Q.T. Do, P. Bernard, Drug Des. Devel. Ther. 4 (2010) 231–242.
[17] P.G. Martins, M. Mori, L.D. Chiaradiadelatorre, A.C. Menegatti, A. Mascarello, B. Botta, J. Benitez, D. Gambino, H. Terenzi, ACS Med. Chem. Lett. 6 (2015) 1035–1040.
[18] L. He, X. Wang, D. Zhu, C. Zhao, W. Du, Metallomics 7 (2015) 1562–1572.
[19] L. Rivillas-Acevedo, C. Sanchez-Lopez, C. Amero, L. Quintanar, Inorg. Chem. 54 (2015) 3788–3796.
[20] A.M. Metelo, R. Perez-Carro, M.M. Castro, P. Lopez-Larrubia, J. Inorg. Biochem. 115 (2012) 44–49.
[21] H. Sakurai, Y. Kojima, Y. Yoshikawa, K. Kawabe, H. Yasui, Coord. Chem. Rev. 226 (2002) 187–198.
[22] T.K. Dobravc, K. Maejima, Y. Yoshikawa, A. Meden, H. Yasui, F. Perdih, New J. Chem. 42 (2018) 3619–3632.
[23] G.R. Willsky, L.H. Chi, G.M. Rd, P.J. Kostyniak, J.J. Smee, A.M. Trujillo, J.A. Alfano, W. Ding, Z. Hu, D.C. Crans, Coord. Chem. Rev. 255 (2011) 2258–2269.
[24] D.C. Crans, A.M. Trujillo, P.S. Pharazyn, M.D. Cohen, Coord. Chem. Rev. 255 (2011) 2178–2192.
[25] X. Yang, K. Wang, J. Lu, D.C. Crans, Coord. Chem. Rev. 237 (2003) 103–111.
[26] D. Rehder, J.C. Pessoa, C.F. Geraldes, M.M. Castro, T. Kabanos, T. Kiss, B. Meier, G. Micera, L. Pettersson, M. Rangel, J. Biol. Inorg. Chem. 7 (2002) 384–396.
[27] H. Sakurai, Chem. Rec. 2 (2002) 237–248.
[28] T. Moroki, Y. Yoshikawa, K. Yoshizawa, A. Tsubura, H. Yasui, Metallomics 6 (2014) 1632–1638.
[29] S. Kowalski, S. Hac, D. Wyrzykowski, A. Zauszkiewicz-Pawlak, I. Inkielewicz-Stępniak, Oncotarget 8 (2017) 60324–60341.
[30] B.H. Zhang, G.S. Hu, D.S. Zhu, W.J. Wang, G.H. Gong, W.H. Du, Acta Phys. -Chim. Sin. 32 (2016) 1810–1818.
[31] L. He, X. Wang, C. Zhao, D. Zhu, W. Du, Metallomics 6 (2014) 1087–1096.
[32] J. Xu, G. Gong, X. Huang, W. Du, J. Inorg. Biochem. 186 (2018) 60–69.
[33] J.D. Knight, J.A. Hebda, A.D. Miranker, Biochemistry 45 (2006) 9496–9508.
[34] D.C. Crans, L. Yang, A. Haase, X. Yang, Met. Ions Life Sci. 18 (2018) 251–279.
[35] A. Abedini, D.P. Raleigh, Protein Eng. Des. Sel. 22 (2009) 453–459.
[36] J.A. Williamson, J.P. Loria, A.D. Miranker, J. Mol. Biol. 393 (2009) 383–396.
[37] R. Kayed, J. Bernhagen, N. Greenfield, K. Sweimeh, H. Brunner, W. Voelter, A. Kapurniotu, J. Mol. Biol. 287 (1999) 781–796.
[38] J. Madine, E. Jack, P.G. Stockley, S.E. Radford, L.C. Serpell, D.A. Middleton, J. Am. Chem. Soc. 130 (2008) 14990–15001.
[39] K. Tenidis, M. Waldner, J. Bernhagen, W. Fischle, M. Bergmann, M. Weber, M.L. Merkle, W. Voelter, H. Brunner, A. Kapurniotu, J. Mol. Biol. 295 (2000) 1055–1071.
[40] B. Konarkowska, J.F. Aitken, J. Kistler, S. Zhang, G.J.S. Cooper, FEBS J. 273 (2006) 3614–3624.
[41] A. Mascioni, F. Porcelli, U. Ilangovan, A. Ramamoorthy, G. Veglia, Biopolymers 69 (2003) 29–41.
[42] S. Luca, W.M. Yau, R. Leapman, R. Tycko, Biochemistry 46 (2007) 13505–13522.
[43] E.T. Jaikaran, C.E. Higham, L.C. Serpell, J. Zurdo, M. Gross, A. Clark, P.E. Fraser, J. Mol. Biol. 308 (2001) 515–525.
[44] R. Laghaei, N. Mousseau, G. Wei, J. Phys. Chem. B 115 (2011) 3146–3154.
[45] R.P. Nanga, J.R. Brender, J. Xu, G. Veglia, A. Ramamoorthy, Biochemistry 47 (2008) 12689–12697.
[46] A. Demuro, E. Mina, R. Kayed, S.C. Milton, I. Parker, C.G. Glabe, J. Biol. Chem. 280 (2005) 17294–17300.
[47] N. Vuletic, C. Djordjevic, J. Chem. Soc. Dalton Trans. 11 (1973) 1137–1141.
[48] K.H. Thompson, B.D. Liboiron, Y. Sun, K.D. Bellman, I.A. Setyawati, B.O. Patrick, V. Karunaratne, G. Rawji, J. Wheeler, K. Sutton, J. Biol. Inorg. Chem. 8 (2003) 66–74.
[49] A.C. Bhasikuttan, J. Mohanty, Chem. Commun. 53 (2017) 2789–2809.
[50] H.A. Ben, M. Hanaki, K. Murakami, K. Irie, H. Isoda, H. Shigemori, Biol. Pharm. Bull. 40 (2017) 238–241.
[51] V.P. Chauhan, I. Ray, A. Chauhan, J. Wegiel, H.M. Wisniewski, Neurochem. Res. 22 (1997) 805–809.
[52] J.H. Byun, H. Kim, Y. Kim, I. Mook-Jung, D.J. Kim, W.K. Lee, K.H. Yoo, Bioorg. Med. Chem. Lett. 18 (2008) 5591–5593.
[53] D. Jiang, X. Li, R. Williams, S. Patel, L. Men, Y. Wang, F. Zhou, Biochemistry 48 (2009) 7939–7947.
[54] N. Lin, H. Chen, H. Zhang, X. Wan, Q. Su, Endocrine 42 (2012) 107–117.
[55] J.J. Meier, R. Kayed, C.Y. Lin, T. Gurlo, L. Haataja, S. Jayasinghe, R. Langen, C.G. Glabe, P.C. Butler, Am. J. Physiol. Endocrinol. Metab. 291 (2006) E1317–E1324.
[56] H. Szentivanyi, R. Stomberg, Acta Chem. Scand. (1983) 553–559. A37.
[57] N.J. Campbell, M.V. Capparelli, W.P. Griffith, A.C. Skapski, Inorg. Chim. Acta 77 (1983) L215–L216.
[58] D. Sanna, P. Buglyo, L. Biro, G. Micera, E. Garribba, Eur. J. Inorg. Chem. 2012 (2012) 1079–1092.
[59] P. Schwendt, J. Tatiersky, L. Krivosudsky, M. Simunekova, Coord. Chem. Rev. 318 (2016) 135–157.
[60] M.R. Maurya, B. Uprety, F. Avecilla, P. Adao, P.J. Costa, Dalton Trans. 44 (2015) 17736–17755.
[61] J.R. Brender, E.L. Lee, M.A. Cavitt, A. Gafni, D.G. Steel, A. Ramamoorthy, J. Am. Chem. Soc. 130 (2008) 6424–6429.
[62] H. Wang, A. Abedini, B. Ruzsicska, D.P. Raleigh, Biochemistry 53 (2014) 5876–5884.
[63] M. Tct, S. A, J. Habchi, S. Chia, G. Meisl, M. Vendruscolo, C.M. Dobson, K. Tpj, Annu. Rev. Phys. Chem. 69 (2018) 273–298.
[64] G. Gong, W. Wang, W. Du, RSC Adv. 7 (2017) 18512–18522.
[65] Q. Wang, J. Guo, P. Jiao, H. Liu, X. Yao, PLoS One 9 (2014) e94796–e94808.
[66] L.S. Roselin, M.S. Lin, P.H. Lin, Y. Chang, W.Y. Chen, Biotechnol. J. 5 (2010) 85–98.
[67] J.J.A.G. Kamps, J. Huang, J. Poater, C. Xu, B.J.G.E. Pieters, A. Dong, J. Min, W. Sherman, T. Beuming, F.M. Bickelhaupt, Nat. Commun. 6 (2015) 8911–8923.
[68] D. Zhu, G. Gong, W. Wang, W. Du, J. Inorg. Biochem. 170 (2017) 109–116.
[69] F. Chiti, C.M. Dobson, Annu. Rev. Biochem. 75 (2006) 333–366.
[70] D.J. Selkoe, J. Hardy, EMBO Mol. Med. 8 (2016) 595–608.
[71] K.A. Conway, S.J. Lee, J.C. Rochet, T.T. Ding, J.D. Harper, R.E. Williamson, L.P. Jr, Ann. N. Y. Acad. Sci. 920 (2000) 42–45.
[72] G. Forloni, N. Angeretti, R. Chiesa, E. Monzani, M. Salmona, O. Bugiani, F. Tagliavini, Nature 362 (1993) 543–546.
[73] P. Arosio, M. Vendruscolo, C.M. Dobson, T.P. Knowles, Trends Pharmacol. Sci. 35 (2014) 127–135.
[74] Y.S. Eisele, C. Monteiro, C. Fearns, S.E. Encalada, R.L. Wiseman, E.T. Powers, J.W. Kelly, Nat. Rev. Drug Discov. 14 (2015) 759–780.
[75] M.N. Haan, Nat. Clin. Pract. Neurol. 2 (2006) 159–166.
[76] N.B. Nillegoda, A.S. Wentink, B. Bukau, Trends Biochem. Sci. 43 (2018) 1–16.
[77] A.Y. Karulin, R. Caspell, M. Dittrich, P. Lehmann, Cells 4 (2015) 96–111.
[78] M.F. Tomasello, A. Sinopoli, F. Attanasio, M.L. Giuffrida, T. Campagna, D. Milardi, G. Pappalardo, Eur. J. Med. Chem. 81 (2014) 442–455.